

# First-passage times to a fractal boundary: local persistence exponent and its log-periodic oscillations

Yilin Ye,<sup>1,\*</sup> Adrien Chaigneau,<sup>1,†</sup> and Denis S. Grebenkov<sup>1,2,‡</sup>

<sup>1</sup>*Laboratoire de Physique de la Matière Condensée (UMR 7643),  
CNRS – Ecole Polytechnique, Institut Polytechnique de Paris, 91120 Palaiseau, France*

<sup>2</sup>*CNRS - Université de Montréal CRM - CNRS,  
6128 succ Centre-Ville, Montréal QC H3C 3J7, Canada*

(Dated: December 2, 2024)

We investigate the statistics of the first-passage time (FPT) to a fractal self-similar boundary of the Koch snowflake. When the starting position is fixed near the absorbing boundary, the FPT distribution exhibits an apparent power-law decay over a broad range of timescales, culminated by an exponential cut-off. By extensive Monte Carlo simulations, we compute the local persistence exponent of the survival probability and reveal its log-periodic oscillations in time due to self-similarity of the boundary. The effect of the starting point onto this behavior is analyzed in depth. Theoretical bounds on the survival probability are derived from the analysis of diffusion in a circular sector. Physical rationales for the refined structure of the survival probability are presented.

Keywords: diffusion, first-passage time, fractal, self-similarity, persistence exponent, survival probability

## I. INTRODUCTION

The statistics of first-passage times (FPTs) to various targets were thoroughly investigated [1–5]. Most former works were dedicated to a common setting when the starting point of the particle is uniformly distributed, in which case the distribution of the FPT is often close to be exponential [6] and thus determined by the mean FPT (MFPT). The latter was studied in depth, especially in the narrow-escape limit when the target is small [7–17]. In this paper, we are interested in a different situation when the particle starts in a vicinity of an absorbing self-similar boundary. Here, the whole boundary plays the role of a sink and thus cannot be treated as a small target so that most formerly used techniques and results are not applicable anymore.

In the simplest case, one can think of diffusion in the upper half-plane towards the absorbing horizontal axis. As lateral displacements are irrelevant due to the translational invariance of the system in this direction, the problem is reduced to fairly classical diffusion in the transverse direction on the positive half-line  $(0, \infty)$  with an absorbing endpoint at 0, for which the survival probability and the probability density function (PDF) of the FPT are explicitly known:

$$S_{1d}(t) = \operatorname{erf}(h_0/\sqrt{4Dt}), \quad (1a)$$

$$H_{1d}(t) = \frac{h_0}{\sqrt{4\pi Dt^3}} e^{-h_0^2/(4Dt)}, \quad (1b)$$

where  $\operatorname{erf}(z)$  is the error function,  $h_0$  is the distance to the absorbing axis, and  $D$  is the diffusion coefficient. In

particular, the survival probability exhibits a power-law decay at long times,  $S_{1d}(t) \propto t^{-\alpha}$ , with the persistence exponent  $\alpha = 1/2$ . In disordered systems, there is no explicit solution like Eq. (1a) but a power-law decay of the survival probability is generally valid (see [18] and references therein). In particular, when the boundary is fractal, the persistence exponent is affected by the geometric irregularity [19] (see also [20]). For instance, in the planar case, the long-time behavior is

$$S(t) \propto t^{-\alpha}, \quad \alpha = d_f/2, \quad (2)$$

where  $d_f$  is the fractal (Minkowski) dimension of the boundary. This result was rigorously obtained when the particle starts uniformly on a contour line at a fixed small distance  $h_0$  from the boundary.

Our goal is to refine the above picture by considering a fixed starting point near the boundary. For this purpose, we study the statistics of the FPT towards a fractal self-similar boundary of the Koch snowflake (Fig. 1). Former studies of diffusion towards fractal boundaries were mainly focused on the spatial distribution of the absorption points (so-called harmonic measure or hitting probabilities) [21–27], that determines, e.g., the growth kinetics of diffusion-limited aggregates [28–30]. We emphasize that our setting is drastically different from diffusion in a disordered fractal medium such as a percolation cluster [31] or a Sierpinski gasket. In the latter case, the fractality of the domain makes the diffusive dynamics anomalous that also impacts the statistics of the FPT [32–47]. In contrast, we consider ordinary diffusion inside a Euclidean (non-fractal) domain (of dimension 2) with a self-similar boundary (of fractal dimension  $1 < d_f < 2$ ). Nevertheless, the behavior of the survival probability and of the MFPT turns out to be much richer than earlier expected. For instance, the (average) persistence exponent depends on the starting point and its neighborhood. Moreover, we reveal a finer structure of the survival probability by evaluating the local persistence exponent. The

\* yilin.ye@polytechnique.edu

† adrien.chaigneau@polytechnique.edu

‡ denis.grebenkov@polytechnique.edu

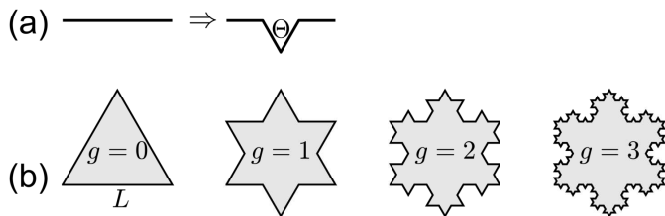


FIG. 1. Iterative construction of the Koch snowflake. **(a)** At each iteration, each linear segment is replaced by a simple generator formed by four equal segments and characterized by the angle  $\Theta = \pi/3$ . **(b)** Starting from the zeroth generation  $g = 0$  (an equilateral triangle with the edges of length  $L$ ), one constructs iteratively next generations.

latter is shown to exhibit log-periodic oscillations in time. In this light, the former universal result (2) turns out to represent an averaged behavior due to the uniform distribution of the starting point.

The paper is organized as follows. In Sec. II, we present analytical results on the FPT distribution in a sector and a wedge. These results will guide us in the analysis of the FPT to the boundary of the Koch snowflake in Sec. III. Section IV concludes the paper.

## II. FIRST-PASSAGE TIMES IN A SECTOR

It is instructive to start the analysis of the FPT distribution for the zeroth generation of the Koch snowflake, namely, the equilateral triangle (Fig. 1). For this domain, the Laplacian eigenfunctions with Dirichlet boundary condition are known explicitly [48–51], which allows one to write spectral expansions for the survival probability and the PDF. However, we prefer to focus on a circular sector of angle  $\Theta$  and radius  $R$ . When  $\Theta = \pi/3$ , this shape is geometrically close to the equilateral triangle so that the FPT distribution exhibits very similar features. In turn, the circular sector gives more flexibility (changing the angle  $\Theta$ ) and more explicit formulas that facilitate their interpretations.

### A. Circular sector

In polar coordinates  $(r, \theta)$ , the sector is defined as

$$\Omega_{\Theta, R} = \{(r, \theta) : 0 < r < R, 0 < \theta < \Theta\}. \quad (3)$$

The eigenvalues and eigenfunctions of the Laplace operator in  $\Omega_{\Theta, R}$  with Dirichlet boundary condition are given by (see [51] for details and references):

$$\lambda_{nk} = \alpha_{nk}^2/R^2, \quad u_{nk} = c_{nk} J_{\nu_n}(\alpha_{nk}r/R) \sin(\nu_n\theta), \quad (4)$$

where  $\nu_n = \pi n/\Theta$  ( $n = 1, 2, 3, \dots$ ),  $\alpha_{nk}$  are the zeros of the Bessel function of the first kind,  $J_{\nu_n}(\alpha_{nk}) = 0$  (enumerated by  $k = 1, 2, 3, \dots$ ), and  $c_{nk}$  are the normalization

coefficients:

$$\begin{aligned} c_{nk}^{-2} &= \int_0^R dr r \int_0^\Theta d\theta [J_{\nu_n}(\alpha_{nk}r/R) \sin(\nu_n\theta)]^2 \\ &= \frac{R^2\Theta}{4} J_{\nu_n+1}^2(\alpha_{nk}). \end{aligned} \quad (5)$$

As a consequence, the survival probability reads

$$\begin{aligned} S_{\Theta, R}(t|\mathbf{x}_0) &= \sum_{n=1}^{\infty} \sum_{k=1}^{\infty} e^{-Dt\lambda_{nk}} u_{nk}(\mathbf{x}_0) \int_{\Omega} d\mathbf{x} u_{nk}(\mathbf{x}) \\ &= \sum_{n=1}^{\infty} \sum_{k=1}^{\infty} e^{-Dt\lambda_{nk}} c_{nk}^2 J_{\nu_n}(\alpha_{nk}r_0/R) \sin(\nu_n\theta_0) \\ &\quad \times \frac{1 - (-1)^n}{\nu_n} R^2 \int_0^1 dx x J_{\nu_n}(\alpha_{nk}x), \end{aligned} \quad (6)$$

where  $\mathbf{x}_0 = (r_0, \theta_0)$  is the starting point in polar coordinates. In turn, the PDF of the FPT is obtained by taking the time derivative:

$$H_{\Theta, R}(t|\mathbf{x}_0) = -\partial_t S_{\Theta, R}(t|\mathbf{x}_0). \quad (7)$$

If the starting point  $\mathbf{x}_0$  is uniformly distributed in  $\Omega$ , one gets

$$\begin{aligned} \overline{S_{\Theta, R}(t)} &= \frac{2}{\Theta R^2} \int_{\Omega} d\mathbf{x}_0 S_{\Theta, R}(t|\mathbf{x}_0) \\ &= \frac{2R^2}{\Theta} \sum_{n=1}^{\infty} \sum_{k=1}^{\infty} e^{-Dt\lambda_{nk}} c_{nk}^2 \\ &\quad \times \left( \frac{1 - (-1)^n}{\nu_n} \int_0^1 dx x J_{\nu_n}(\alpha_{nk}x) \right)^2. \end{aligned} \quad (8)$$

In turn, the MFPT can be found as

$$\begin{aligned} T_{\Theta, R}(\mathbf{x}_0) &= \int_0^{\infty} dt t H_{\Theta, R}(t|\mathbf{x}_0) = \int_0^{\infty} dt S_{\Theta, R}(t|\mathbf{x}_0) \\ &= \frac{R^2}{D} \sum_{n=1}^{\infty} \sum_{k=1}^{\infty} \frac{c_{nk}^2}{\lambda_{nk}} J_{\nu_n}(\alpha_{nk}r_0/R) \sin(\nu_n\theta_0) \\ &\quad \times \frac{1 - (-1)^n}{\nu_n} \int_0^1 dx x J_{\nu_n}(\alpha_{nk}x). \end{aligned} \quad (9)$$

One can further simplify this expression by using the summation identities for series with Bessel functions [52, 53]. In particular, the Kneser-Sommerfeld expansion gives

$$\sum_{k=1}^{\infty} \frac{J_{\nu}(\alpha_{\nu, k}z) J_{\nu}(\alpha_{\nu, k}z_0)}{\alpha_{\nu, k}^2 J_{\nu+1}^2(\alpha_{\nu, k})} = \frac{z^{\nu}}{4\nu} (z_0^{-\nu} - z_0^{\nu}) \quad (10)$$

for  $0 \leq z \leq z_0 \leq 1$  (see, e.g., Eq. (D10) from Table 3 in [53]; note that the factor  $\pi/2$  was missing in the right-hand side of Eq. (D10)). As a consequence, we have

$$\begin{aligned}
T_{\Theta,R} &= \frac{R^2}{D\Theta} \sum_{n=1}^{\infty} \frac{1 - (-1)^n}{\nu_n} \sin(\nu_n \theta_0) \frac{1}{\nu_n} \left\{ \int_0^{z_0} dz z z^{\nu_n} (z_0^{-\nu_n} - z^{\nu_n}) + \int_{z_0}^1 dz z z_0^{\nu_n} (z^{-\nu_n} - z^{\nu_n}) \right\} \\
&= \frac{R^2}{D\Theta} \sum_{n=1}^{\infty} \frac{1 - (-1)^n}{\nu_n^2} \sin(\nu_n \theta_0) \left\{ \frac{z_0^{\nu_n+2}}{\nu_n+2} (z_0^{-\nu_n} - z_0^{\nu_n}) + z_0^{\nu_n} \left( \frac{1 - z_0^{2-\nu_n}}{2 - \nu_n} - \frac{1 - z_0^{2+\nu_n}}{2 + \nu_n} \right) \right\} \\
&= \frac{2R^2}{D\Theta} \sum_{n=1}^{\infty} \frac{1 - (-1)^n}{\nu_n} \sin(\nu_n \theta_0) \frac{z_0^2 - z_0^{\nu_n}}{\nu_n^2 - 4}, \tag{11}
\end{aligned}$$

where  $z_0 = r_0/R$ . One can rewrite it as

$$T_{\Theta,R} = T_{\Theta,\infty} - \frac{2R^2}{D\Theta} \sum_{n=1}^{\infty} \frac{1 - (-1)^n}{\nu_n(\nu_n^2 - 4)} \sin(\nu_n \theta_0) (r_0/R)^{\nu_n}, \tag{12}$$

where

$$T_{\Theta,\infty} = \frac{r_0^2}{4D} \left( \frac{\cos(2\theta_0 - \Theta)}{\cos \Theta} - 1 \right). \tag{13}$$

We could not find earlier references with an explicit form (12) for the MFPT in a sector. When  $\Theta < \pi/2$ , the expression (13) can be interpreted as the MFPT to the wedge of angle  $\Theta$  (or infinite sector with  $R = \infty$ ) that was discussed in [54]. In turn, if  $\Theta \geq \pi/2$ , the MFPT to the wedge is infinite (see below), whereas Eq. (13) yields negative values. At the same time, Eq. (12) is valid for any  $\Theta$  from 0 to  $2\pi$ .

This important result unveils the scaling of the MFPT with respect to  $r_0$ . As  $r_0 \rightarrow 0$ , the sum in Eq. (12) scales in the leading order as  $r_0^{\pi/\Theta}$ , whereas  $T_{\Theta,\infty}$  scales as  $r_0^2$ . Depending on  $\Theta$ , one of these two contributions is dominant, implying

$$\frac{D}{R^2} T_{\Theta,R} \approx \begin{cases} \frac{1}{4} \left( \frac{\cos(2\theta_0 - \Theta)}{\cos \Theta} - 1 \right) (r_0/R)^2 & (\Theta < \pi/2), \\ \frac{\sin(2\theta_0)}{\sin(\pi/2)} (r_0/R)^2 \ln(R/r_0) & (\Theta = \pi/2), \\ \frac{\Theta^2 \pi}{\pi(\Theta^2 - \pi^2/4)} (r_0/R)^{\pi/\Theta} & (\Theta > \pi/2) \end{cases} \tag{14}$$

(in the border case  $\Theta = \pi/2$ , both contributions are comparable so that one has to use directly Eq. (11) to get the logarithmic correction). The exact form of the second moment of the FPT and the discussion on its variance are reported in Appendix A.

Figure 2 shows the behavior of  $T_{\Theta,R}$  as a function of  $r_0$  and illustrates the accuracy of the asymptotic relations (14). As the MFPT vanishes in the limits  $r_0 = 0$  and  $r_0 = R$ , there is an optimal location of the starting point that maximizes  $T_{\Theta,R}$  with respect to  $r_0$ . In the considered case when the starting point is on the middle ray (i.e.,  $\theta_0 = \Theta/2$ ), one sees that the optimal value  $r_0^*$ , at which the MFPT is maximal, decreases as  $\Theta$  increases (i.e., the maximum of the MFPT shifts to the left). Indeed, the MFPT is expected to be larger when the starting point is further from the boundary. For the

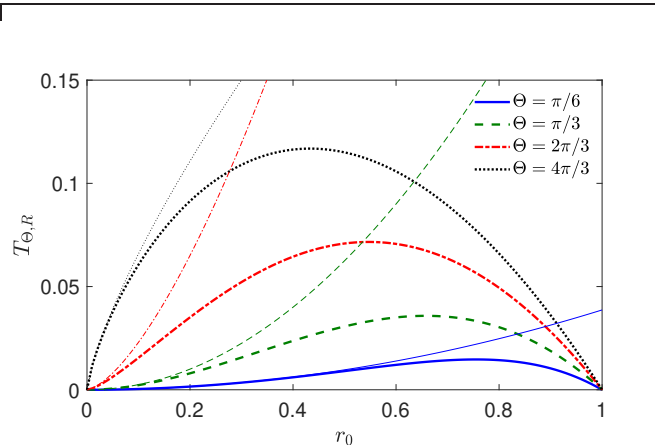


FIG. 2. MFPT  $T_{\Theta,R}$  in sectors of different angles  $\Theta$ , with  $\theta_0 = \Theta/2$  and variable  $r_0$ . Thin lines present the asymptotic relations (14). We set  $D = 1$  and  $R = 1$ .

starting point on the middle ray, the largest distance to the boundary is achieved from the center of the incircle (i.e., the largest circle inscribed into the circular sector). Its radius  $\rho$  can be found by setting  $\rho = r_0^* \sin(\Theta/2)$  and  $r_0^* + \rho = R$ , from which  $\rho = R \sin(\Theta/2)/(1 + \sin(\Theta/2))$  and thus  $r_0^* = R/(1 + \sin(\Theta/2))$  for  $\Theta \leq \pi$ . For instance, we get  $r_0^* \approx 0.79, 0.67, 0.54$  at  $\Theta = \pi/6, \pi/3, 2\pi/3$ , respectively, which are in excellent agreement with the positions of the maxima shown in Fig. 2. For any  $\Theta > \pi$ , the inradius  $\rho$  remains equal to  $1/2$ , so that the optimal position  $r_0^*$  is also located around 0.5. Note that these extremal properties are not captured by the asymptotic relations (14).

## B. Wedge case

For the wedge of angle  $\Theta$  (i.e., the infinite sector with  $R = \infty$ ), one can get an explicit solution for the propagator and the survival probability (see [54–57] and references therein):

$$S_{\Theta,\infty}(t|\mathbf{x}_0) = 2 \sum_{n=1}^{\infty} \frac{1 - (-1)^n}{\pi n} \sin(\nu_n \theta_0) R_{\nu_n}(r_0/\sqrt{Dt}), \tag{15}$$

where

$$R_\nu(z) = \frac{\sqrt{\pi}}{4} z e^{-z^2/8} \left( I_{\nu-1/2}(z^2/8) + I_{\nu+1/2}(z^2/8) \right), \quad (16)$$

with  $I_\nu(z)$  being the modified Bessel function of the first kind (when the wedge angle has a special form,  $\Theta = \pi/m$ , with an integer  $m$ , the above expression can be further simplified, see [58], as well as [59] for an extension). Note that  $R_\nu(z) \rightarrow 1$  as  $z \rightarrow \infty$  so that  $S_{\Theta,\infty}(t|\mathbf{x}_0)$  approaches 1 as  $t \rightarrow 0$ , as it should. In turn, in the long-time limit, one retrieves the power-law decay [1]

$$S_{\Theta,\infty}(t|\mathbf{x}_0) \propto (r_0/\sqrt{Dt})^{\pi/\Theta} \quad (t \gg r_0^2/D), \quad (17)$$

with the persistence exponent  $\alpha = \pi/(2\Theta)$ . As a consequence, the MFPT is infinite for  $\Theta \geq \pi/2$  and finite for  $\Theta < \pi/2$  (see Eq. (13)). The negative derivative of  $S_{\Theta,\infty}(t|\mathbf{x}_0)$  with respect to  $t$  yields the probability density function of the FPT to the wedge boundary:

$$H_{\Theta,\infty}(t|\mathbf{x}_0) = \frac{r_0}{\sqrt{Dt^3}} \sum_{n=1}^{\infty} \frac{1 - (-1)^n}{\pi n} \times \sin(\nu_n \theta_0) R'_{\nu_n}(r_0/\sqrt{Dt}), \quad (18)$$

where

$$R'_\nu(z) = \frac{\sqrt{\pi}}{4} \nu e^{-z^2/8} \left( I_{\nu-1/2}(z^2/8) - I_{\nu+1/2}(z^2/8) \right) \quad (19)$$

is the derivative of  $R_\nu(z)$ .

### C. Three distinct regimes

Figure 3 illustrates the behavior of the survival probability and the PDF of the FPT for the sector of angle  $\Theta = \pi/3$  and radius  $R = 1$ . We choose the starting point  $\mathbf{x}_0 = (r_0, \theta_0)$  to be located near the horizontal segment of the sector in the vicinity of its vertex (with  $r_0 = 10^{-2}$  and  $\theta_0 = 10^{-2}$  so that the initial distance to the boundary,  $h_0 = r_0 \sin \theta_0 \approx 10^{-4}$ , is the smallest lengthscale). This choice helps to illustrate three distinct regimes:

(i) At short times,  $t \ll r_0^2/D$ , the particle diffuses near the absorbing horizontal segment, as if it was in the upper half-plane above the absorbing horizontal line. In this regime, the survival probability and the PDF are determined by diffusion in the transverse direction on the semi-axis  $(0, +\infty)$  with the absorbing endpoint, so that  $S_{\Theta,R}(t|\mathbf{x}_0) \approx S_{1d}(t)$  and  $H_{\Theta,R}(t|\mathbf{x}_0) \approx H_{1d}(t)$ , given by Eqs. (1). This short-time behavior, which is shown by a dash-dotted line, is universal (see [60, 61] for more discussions). In particular, if  $h_0^2/D \ll t \ll r_0^2/D$ , one has  $S_{\Theta,R}(t|\mathbf{x}_0) \approx h_0/\sqrt{\pi Dt}$ . Note also that the maximum of the Lévy-Smirnov density in the right-hand side of Eq. (1b) is realized at  $t_{\text{mp}} = h_0^2/(6D)$ . In this setting, one sees that the most probable FPT in the sector is well approximated by that  $t_{\text{mp}}$ .

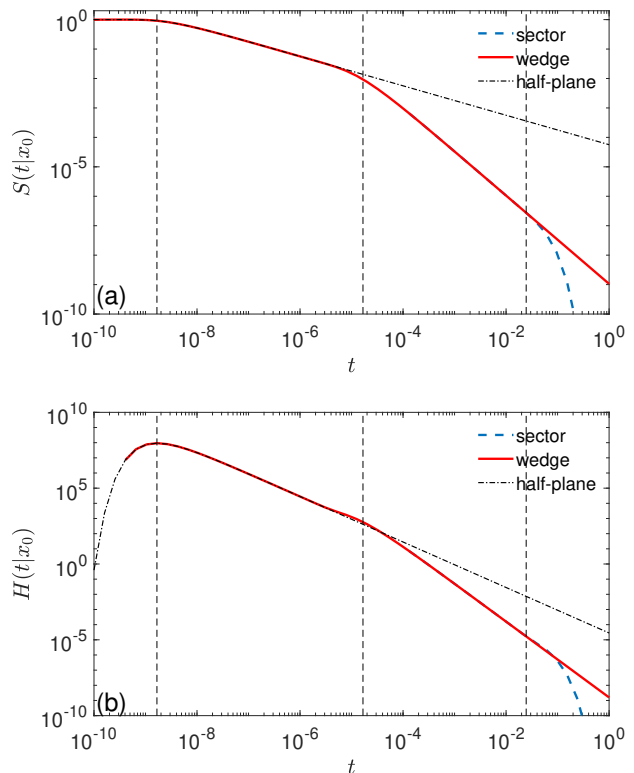


FIG. 3. (a) Survival probability  $S_{\Theta,R}(t|\mathbf{x}_0)$  in a circular sector of angle  $\Theta = \pi/3$  and radius  $R = 1$ , with the starting point  $\mathbf{x}_0 = (r_0, \theta_0) = (10^{-2}, 10^{-2})$  in polar coordinates, and  $D = 1$ . This survival probability, which is shown by thick dashed line, was obtained by truncating the double series in Eq. (6) to 7354 terms to enable its accurate computation even at very short times. It is compared to  $S_{\Theta,\infty}(t|\mathbf{x}_0)$  for the wedge (thick solid line, Eq. (15)) and to  $S_{1d}(t)$  in the half-plane (thin dash-dotted line, Eq. (1a)). (b) PDF  $H_{\Theta,R}(t|\mathbf{x}_0)$  in the same sector (shown by thick dashed line) was also computed from its truncated spectral expansion; it is compared to  $H_{\Theta,\infty}(t|\mathbf{x}_0)$  (thick solid line, Eq. (18)) and  $H_{1d}(t)$  (dash-dotted line, Eq. (1b)). Three vertical dashed lines indicate three timescales:  $h_0^2/(6D)$ ,  $r_0^2/(6D)$ , and  $1/(D\lambda_{\min}) \approx 0.025 R^2/D$ , where  $h_0 = r_0 \sin \theta_0 \approx 10^{-4}$ .

(ii) At intermediate times,  $r_0^2/D \lesssim t \ll R^2/D$ , the particle is confined within an absorbing angle that affects its survival. In turn, it does not “feel” the presence of the arc of the sector (located at distance  $R$ ), as if it diffused in an infinite wedge. As a consequence, the survival probability and the PDF of the FPT for the sector are very close to that for the wedge (shown by solid lines). Figure 3 confirms the remarkable agreement between these quantities over intermediate times. In particular, one observes the power-law asymptotic decay (17) at  $r_0^2/D \ll t \ll R^2/D$ .

(iii) At long times,  $t \gtrsim R^2/D$ , the particle explores the whole sector and thus starts to “feel” the confinement by the absorbing arc. The confinement inside a bounded domain changes the previous power-law regime,

$S_{\Theta,R}(t|\mathbf{x}_0) \propto t^{-\pi/(2\Theta)}$ , into an exponential cut-off, which is determined by the smallest eigenvalue  $\lambda_{\min}$  of the Laplace operator:  $\lambda_{\min} = \alpha_{1,1}^2/R^2$ , where  $\alpha_{1,1}$  is the smallest positive zero of the Bessel function  $J_{\pi/\Theta}(z)$ . In fact, when  $t \gg R^2/D$ , one has  $S_{\Theta,R}(t|\mathbf{x}_0) \propto e^{-Dt\lambda_{\min}}$ . For  $\Theta = \pi/3$ , one gets  $\alpha_{1,1} \approx 6.3802$  that determines the decay rate  $1/(D\lambda_{\min}) \approx 0.025R^2/D$ .

The three relevant timescales revealed in the above analysis are naturally related to three lengthscales: the distance  $h_0$  to the flat boundary, the distance  $r_0$  to a singularity (the angle), and the radius  $R$  of the sector. As a consequence, the timespans of the three regimes depend on the location of the starting point. For instance, changing  $\theta_0$  from  $10^{-2}$  to, say,  $\pi/6$  (the middle ray of the sector) can eliminate the first regime (as  $h_0$  becomes comparable to  $r_0$ ), whereas changing  $r_0$  from  $10^{-2}$  to, say,  $0.5$  can eliminate the second regime (as  $r_0$  becomes comparable to  $R$ ). Finally, if the starting point is located somewhere in the middle of the sector, both first and second regimes can be effectively removed. In the same vein, if the starting point is uniformly distributed in the sector, the first two regimes become irrelevant. In this uniform setting, the MFPT is close to the decay rate that determines the exponential cut-off, whereas the FPT obeys approximately an exponential law [6]. Most former works dealt with this setting and focused on the MFPT as the unique relevant timescale. The aim of the present paper is to investigate the opposite situation when the particle starts in a vicinity of the absorbing boundary, in which case the FPT distribution is much richer.

### III. FIRST-PASSAGE TIMES IN THE KOCH SNOWFLAKE

Despite the geometric simplicity of the sector domain, the three regimes discussed in Sec. II capture the generic features of the FPT distribution. When the sector is replaced by a polygon, the first and the third regimes remain unchanged. Indeed, if the particle starts very close to the boundary, one still deals with diffusion near a segment at very short times, so that Eqs. (1) provide accurate approximations for  $S(t|\mathbf{x}_0)$  and  $H(t|\mathbf{x}_0)$ . Moreover, the exponential cut-off is also present at very long times due to confinement in a bounded domain. Both limits are rather basic and well understood. For instance, several studies focused on the smallest eigenvalue  $\lambda_{\min}$  of the Laplace operator in domains with fractal boundary (see [62–66] and references therein) that determines the decay time of the exponential cut-off (see below). Our main emphasis is therefore on the intermediate regime. For this purpose, we choose the starting point to be at distance  $h_0$  from the boundary such that

$$\ell_g \ll h_0 \ll L, \quad (20)$$

where  $L$  is the size of the domain, and  $\ell_g$  is the length of the smallest segment used for constructing the prefractal boundary of generation  $g$ , as explained below.

#### A. Koch snowflake

To enable efficient numerical simulations, we consider diffusion in the Koch snowflake that is constructed iteratively from a simple generator with a chosen angle  $\Theta$  (Fig. 1a). One starts from an equilateral triangle  $\Omega_0$  with edges of length  $L$  that is referred to as the generation 0. Each linear segment of the boundary  $\partial\Omega_0$  is replaced by rescaled and appropriately rotated generator to produce the first generation  $\Omega_1$ . Its boundary  $\partial\Omega_1$  is composed of  $3 \cdot 4 = 12$  segments of length  $\ell_1 = L/(2[1 + \sin(\Theta/2)])$ . In the same way, one constructs iteratively the successive generations  $\Omega_2, \Omega_3, \dots$  of the Koch snowflake (Fig. 1b). The boundary  $\partial\Omega_g$  is composed of  $3 \cdot 4^g$  segments of length

$$\ell_g = \frac{L}{(2[1 + \sin(\Theta/2)])^g}. \quad (21)$$

The boundary  $\partial\Omega_\infty$  of the limiting domain  $\Omega_\infty$  is fractal; in particular, it is not differentiable and has infinite length (in fact, the perimeter of  $\partial\Omega_g$ ,  $3 \cdot 4^g \ell_g$ , diverges as  $g \rightarrow \infty$ ). By a scaling argument, the fractal dimension of  $\partial\Omega_\infty$  is

$$d_f = \frac{\ln(4)}{\ln(2[1 + \sin(\Theta/2)])}, \quad (22)$$

and it ranges from 1 at  $\Theta = \pi$  to 2 as  $\Theta \rightarrow 0$ . This family of Koch snowflakes is therefore convenient for studying the effect of a self-similar absorbing boundary onto the FPT distribution. Throughout this paper, we focus on the canonical Koch snowflake with  $\Theta = \pi/3$  so that  $\ell_g = L/3^g$  and  $d_f = \ln(4)/\ln(3) \approx 1.262$ .

We study the distribution of the FPT,  $\mathcal{T}_g$ , to the boundary  $\partial\Omega_g$  of the  $g$ -th generation  $\Omega_g$ . The associated survival probability and the PDF are denoted as  $S_g(t|\mathbf{x}_0) = \mathbb{P}_{\mathbf{x}_0}\{\mathcal{T}_g > t\}$  and  $H_g(t|\mathbf{x}_0) = -\partial_t S_g(t|\mathbf{x}_0)$ , respectively. Note that these quantities also determine all the moments of the FPT, which are finite for any bounded domain  $\Omega_g$ ; for instance, the MFPT is

$$\langle \mathcal{T}_g \rangle_{\mathbf{x}_0} = \int_0^\infty dt t H_g(t|\mathbf{x}_0) = \int_0^\infty dt S_g(t|\mathbf{x}_0). \quad (23)$$

#### B. Description of Monte Carlo simulations

In order to estimate these quantities, we employ the geometry-adapted fast random walk algorithm [25, 26], which combines the standard walk-on-spheres method by Muller [67] and self-similar structure of the Koch snowflake for a rapid evaluation of the distance to the boundary. For a given  $g$ , a random trajectory starts from a fixed point  $\mathbf{x}_0$  and continues until the distance to the boundary  $\partial\Omega_g$  becomes smaller than a prescribed (very small) threshold  $\epsilon$ . The duration of such a trajectory approximates the FPT to the absorbing boundary

$\partial\Omega_g$ . Repeating this simulation  $N$  times, one gets an empirical statistics of the FPT that allows one to estimate both  $S_g(t|\mathbf{x}_0)$  and  $H_g(t|\mathbf{x}_0)$ . For all simulations, we used  $\epsilon = 10^{-10}$  to ensure very accurate approximation of the FPT even for large  $g$ , and  $N = 10^8$  to get a sufficient statistics for estimating  $S_g(t|\mathbf{x}_0)$  and  $H_g(t|\mathbf{x}_0)$ . In order to get more accurate statistics of rare realizations of large FPTs, we also performed additional simulations, in which the generated FPT  $\mathcal{T}_g$  below a prescribed time  $T_{\min}$  were discarded to accumulate  $N = 10^8$  realizations of the FPT above  $T_{\min}$ . A home-built code was written in Fortran90. Numerous datasets of simulated FPTs were recorded for different generations  $g$  and starting points  $\mathbf{x}_0$ . Each dataset was then analyzed in Matlab by using the standard routines `ecdf` and `hist` for getting the empirical cumulative distribution function (CDF) and the histogram (the latter was then rescaled into an empirical PDF). As the distribution of the FPT  $\mathcal{T}_g$  is very broad, we actually produced the histogram of  $\ln(\mathcal{T}_g)$  and then transformed it into the histogram of  $\mathcal{T}_g$ . Throughout this section, we fix length and time units by setting  $L = 2$  and  $D = 1$ .

For the zeroth generation  $\Omega_0$  (i.e., the equilateral triangle of lengthside  $L = 2$ ), the smallest eigenvalue of the Dirichlet Laplacian is known exactly:  $\lambda_{\min} = 4\pi^2/3 \approx 13.16$ , see [49]. As  $g$  increases,  $\lambda_{\min}$  decreases and rapidly converges to a well-defined limit. Banjai computed numerically the smallest eigenvalue of the Laplace operator for various generations and showed that it changes very little for  $g \geq 4$  (see Table 1 in [66]). His numerical result yields  $\lambda_{\min} \simeq 9.837$  for our setting with  $L = 2$ . This value determines the confinement timescale:

$$t_c = \frac{1}{D\lambda_{\min}} \approx 0.1. \quad (24)$$

### C. MFPT

We start by evaluating the MFPT as a function of the distance  $r_0$  to a chosen vertex of the boundary. For this purpose, we choose a ray in the middle of the angle and change the distance  $r_0$  to the vertex, as illustrated on Fig. 4(b,c). Panels (a) and (b) of Fig. 5 show the dependence of the MFPT on  $r_0$  for two vertices of angles  $4\pi/3$  and  $\pi/3$ , respectively. In both cases, one sees that the MFPT is close to  $T_{\Theta,R}(t|\mathbf{x}_0)$  in the sector and thus inherits its power-law scaling,  $\langle \mathcal{T}_g \rangle_{\mathbf{x}_0} \propto r_0^\beta$ , with  $\beta = 3/4$  and  $\beta = 2$  for two considered cases, respectively. The dependence of the MFPT on the generation  $g$  is rather weak.

### D. Theoretical bounds

Let us now switch to the analysis of the survival probability and first discuss a simple way to get its theoretical bounds. Let  $S(t|\mathbf{x}_0)$  and  $S'(t|\mathbf{x}_0)$  denote the survival probabilities in two domains  $\Omega$  and  $\Omega'$  such that

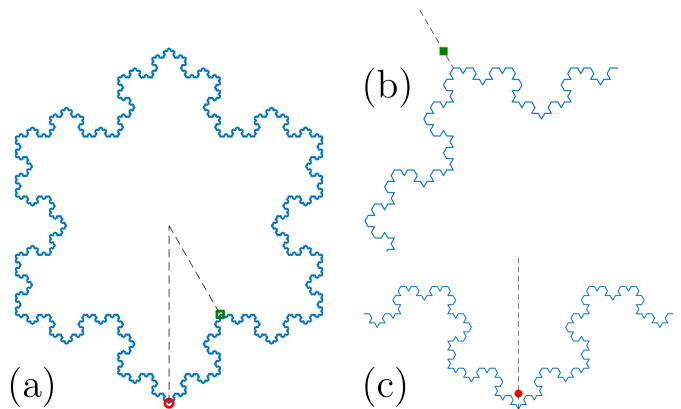


FIG. 4. (a) The 10th generation of the Koch snowflake. Circle and square indicate two starting points close to two vertices of angles  $\pi/3$  and  $4\pi/3$ , respectively. (b,c) Two panels on the right show a zoom around each of these starting points.

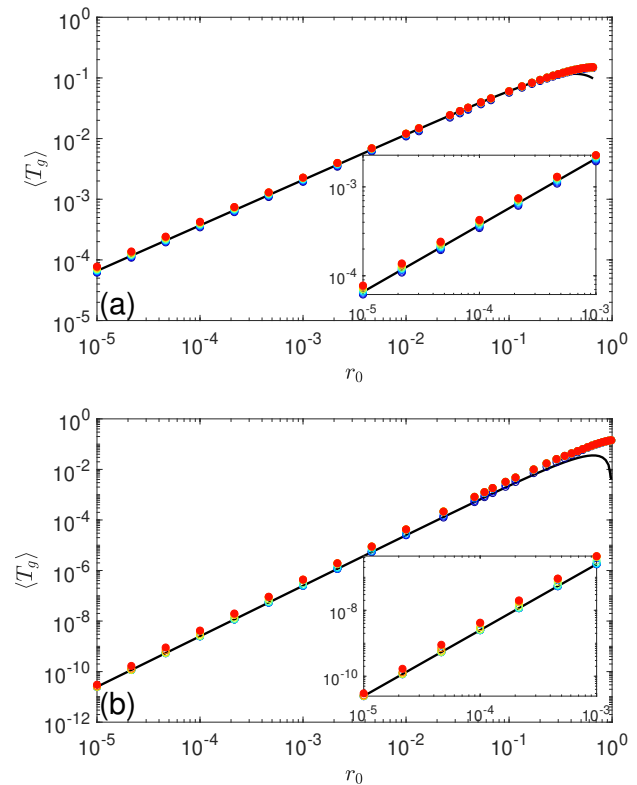


FIG. 5. MFPT as a function of the distance  $r_0$  to a chosen vertex of the boundary, for different generation of the Koch snowflake. (a) Approaching a vertex of angle  $4\pi/3$ , see Fig. 4(b); (b) approaching a vertex of angle  $\pi/3$ , see Fig. 4(c). Solid line presents the MFPT  $T_{\Theta,R}(t|\mathbf{x}_0)$  in the sector of radius  $R = 1$  that exhibits the small- $r_0$  scaling behaviors  $r_0^{3/4}$  (panel (a)) and  $r_0^2$  (panel (b)). Color of symbols changes from dark blue ( $g = 1$ ) to red ( $g = 10$ ), the last one being filled. Insets zoom the regions of small  $r_0$ .

$\mathbf{x}_0 \in \Omega' \subset \Omega$ . Any random trajectory that started from  $\mathbf{x}_0$  and has reached the boundary  $\partial\Omega$  must hit or cross the boundary  $\partial\Omega'$  of the smaller enclosed domain  $\Omega'$ . As a consequence, the FPT  $\tau'$  to  $\partial\Omega'$  is *shorter* than the FPT  $\tau$  to  $\partial\Omega$ . More rigorously, the probabilistic event  $\{\tau' > t\}$  is included into the probabilistic event  $\{\tau > t\}$ , and thus

$$S'(t|\mathbf{x}_0) \leq S(t|\mathbf{x}_0) \quad \text{for any } t \geq 0. \quad (25)$$

The integral of this inequality over  $t$  yields the intuitively expected inequality  $\langle \tau' \rangle \leq \langle \tau \rangle$ , i.e., the MFPT  $\langle \tau' \rangle$  to the smaller enclosed boundary  $\partial\Omega'$  is smaller than the MFPT  $\langle \tau \rangle$  to the larger boundary  $\partial\Omega$ .

For instance, if  $\Omega'$  and  $\Omega$  are two sectors of the same angle  $\Theta$  and radii  $R' < R$ , the survival probability in the shorter sector is smaller:  $S_{\Theta, R'}(t|\mathbf{x}_0) \leq S_{\Theta, R}(t|\mathbf{x}_0)$ . Moreover, if  $\Omega$  is the wedge of the angle  $\Theta$ , then the survival probability  $S_{\Theta, \infty}(t|\mathbf{x}_0)$  in the wedge, given by Eq. (15), is the upper bound for the survival probability  $S_{\Theta, R}(t|\mathbf{x}_0)$  in the sector (and also for the equilateral triangle). Accordingly, the MFPT in the wedge, given by Eq. (13), is the upper bound for the MFPT in the sector, given by Eq. (12). In the same vein, since  $\Omega_{g-1} \subset \Omega_g$ , one also has

$$S_{g-1}(t|\mathbf{x}_0) \leq S_g(t|\mathbf{x}_0) \quad \Rightarrow \quad \langle \mathcal{T}_{g-1} \rangle_{\mathbf{x}_0} \leq \langle \mathcal{T}_g \rangle_{\mathbf{x}_0}. \quad (26)$$

Similarly, one can inscribe a circular sector of angle  $\Theta$  and radius  $R$  into  $\Omega_g$  to get a *lower bound* for  $S_g(t|\mathbf{x}_0)$ :

$$S_{\Theta, R}(t|\mathbf{x}_0) \leq S_g(t|\mathbf{x}_0) \quad \text{for any } t \geq 0, \quad (27)$$

where the largest possible radius is  $R = L\sqrt{7}/3$  for  $\Theta = \pi/3$  (Fig. 6). Moreover, if  $\mathbf{x}_0$  lies close to the vertex of angle  $\Theta$ , i.e.,  $r_0 \ll R$ , the survival probability  $S_{\Theta, R}(t|\mathbf{x}_0)$  can be accurately approximated by  $S_{\Theta, \infty}(t|\mathbf{x}_0)$  for the wedge, at least for intermediate times  $t \ll L^2/D$ .

At the same time, the Koch snowflake can be inscribed into a larger wedge of angle  $\Theta' = (\pi + \Theta)/2$  (Fig. 6). As a consequence, the survival probability  $S_{\Theta', \infty}(t|\mathbf{x}_0)$  for the larger wedge is an upper bound for  $S_g(t|\mathbf{x}_0)$ :

$$S_g(t|\mathbf{x}_0) \leq S_{\Theta', \infty}(t|\mathbf{x}_0). \quad (28)$$

### E. Survival probability and PDF

We first consider the starting point  $\mathbf{x}_0$  close to a vertex of angle  $\pi/3$  on the boundary. For convenience, we keep using local polar coordinates,  $\mathbf{x}_0 = (r_0, \theta_0)$ , which are centered at the chosen vertex of the boundary. We set  $r_0 = 10^{-4}$  and  $\theta_0 = \pi/6$ , i.e., the starting point  $\mathbf{x}_0$  lies on the ray in the middle of the vertex, as illustrated on Fig. 4(c). The survival probability  $S_g(t|\mathbf{x}_0)$  for two generations  $g = 5$  and  $g = 10$ , as well as  $S_{\pi/3, \infty}(t|\mathbf{x}_0)$  and  $S_{2\pi/3, \infty}(t|\mathbf{x}_0)$ , are shown in Fig. 7(a). For  $g = 5$ , the length  $\ell_5 = L(1/3)^5 \approx 8.2 \cdot 10^{-3}$  of

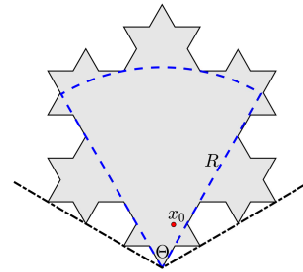


FIG. 6. The second generation of the Koch snowflake of angle  $\Theta = \pi/3$  and  $L = 2$ , with the largest inscribed sector of radius  $R = L\sqrt{7}/3$  (blue dashed line) and the larger wedge of angle  $\Theta' = 2\pi/3$  (black dash-dotted line). Red circle indicates the starting point  $\mathbf{x}_0$ .

the segments considerably exceeds the starting distance  $h_0 = r_0 \sin(\pi/6) = 0.5 \cdot 10^{-4}$  to the boundary. As a consequence, the survival probability  $S_5(t|\mathbf{x}_0)$  is very close to that of the wedge of angle  $\pi/3$ , as confirmed by the figure, with the persistence exponent  $\alpha = \pi/(2\Theta) = 3/2$ . In contrast, for  $g = 10$ , one has  $\ell_{10} = L(1/3)^{10} \approx 3.4 \cdot 10^{-5}$ , which is much smaller than the initial distance. As the inequalities (20) are now satisfied, one can expect the emergence of a nontrivial intermediate regime. Indeed, we observe deviations of the survival probability  $S_{10}(t|\mathbf{x}_0)$  from its lower bound  $S_{\pi/3, R}(t|\mathbf{x}_0) \approx S_{\pi/3, \infty}(t|\mathbf{x}_0)$ . Note also that the upper bound given by the survival probability  $S_{2\pi/3, \infty}(t|\mathbf{x}_0)$  (with the persistence exponent  $\pi/(2\Theta') = 3/4$ ) is not tight. Fitting  $S_{10}(t|\mathbf{x}_0)$  by a power law over an intermediate range of times gives the persistence exponent close to 1.25. This value is smaller than the persistence exponent  $3/2$  of the wedge, but larger than the persistence exponent  $d_f/2 \approx 0.63$  predicted in [19] (see further discussions in Sec. III F). The associated PDFs are illustrated on Fig. 7(b). We emphasize on a very broad range of relevant timescales, ranging from  $t_{\text{mp}} \approx h_0^2/(6D) \approx 4 \cdot 10^{-10}$  to  $t_c \approx 10^{-1}$ , see Eq. (24). Note that the exponential cut-off determined by  $t_c$ , is not shown here due to insufficient accuracy of the empirical statistics for very large FPTs.

The behavior is quite different for the starting point near the angle  $4\pi/3$ , illustrated on Fig. 4(b). Figure 8(a) indicates that the survival probabilities  $S_5(t|\mathbf{x}_0)$  and  $S_{10}(t|\mathbf{x}_0)$  are close to each other and to the survival probability  $S_{4\pi/3, \infty}(t|\mathbf{x}_0)$  for the wedge of angle  $4\pi/3$ , which exhibits the power-law decay with the persistence exponent  $\alpha = \pi/(2\Theta) = 3/8$ . Quite remarkably,  $S_{4\pi/3, \infty}(t|\mathbf{x}_0)$  turns out to be an accurate approximation for a broad range of times, up to  $10^{-1}$ . At this timescale, the particle starts to feel the confinement, as witnessed by the expected exponential cut-off. A similar behavior is found for the PDF  $H_g(t|\mathbf{x}_0)$  shown on Fig. 8(b).

We conclude that the power-law decay of the survival probability near the Koch snowflake strongly depends on the location of the starting point; in particular, the persistence exponent can considerably vary, e.g., by taking

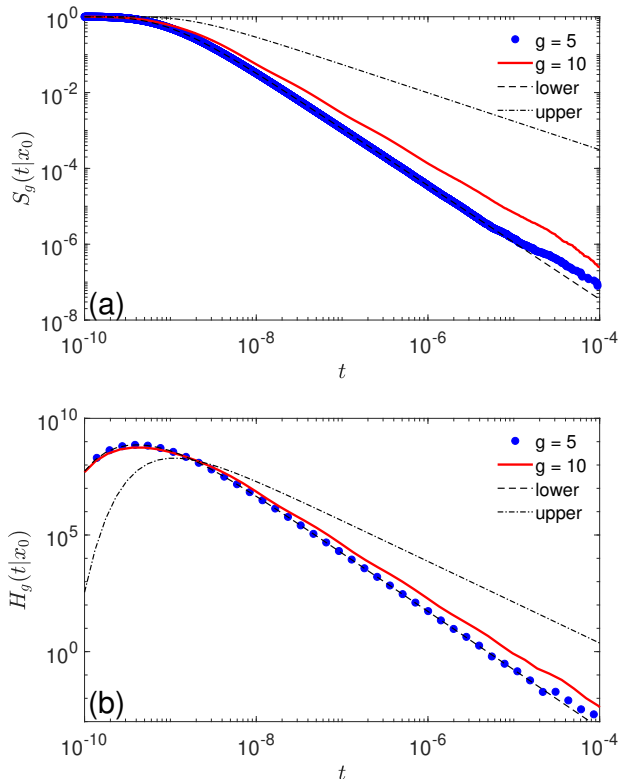


FIG. 7. (a) Survival probability  $S_g(t|\mathbf{x}_0)$  and (b) PDF  $H_g(t|\mathbf{x}_0)$  for two generations  $g = 5$  (circles) and  $g = 10$  (solid line) of the Koch snowflake with  $\Theta = \pi/3$ ,  $L = 2$ ,  $D = 1$ ,  $r_0 = 10^{-4}$  and  $\theta_0 = \Theta/2$ , starting near the angle  $\pi/3$  (Fig. 4(c)), obtained by Monte Carlo simulations with  $N = 10^8$  particles. Thin lines show the survival probabilities  $S_{\pi/3,\infty}(t|\mathbf{x}_0)$  and  $S_{2\pi/3,\infty}(t|\mathbf{x}_0)$  for the wedges of angles  $\pi/3$  (dashed line) and  $2\pi/3$  (dash-dotted line) on panel (a), and the associated PDFs  $H_{\pi/3,\infty}(t|\mathbf{x}_0)$  and  $H_{2\pi/3,\infty}(t|\mathbf{x}_0)$  on panel (b).

a value of 1.25 in the vicinity of the angle  $\pi/3$  and 0.38 near the angle  $4\pi/3$ . How is it possible that the long-time behavior of the survival probability is so sensitive to the starting point? Indeed, large FPTs correspond to the random trajectories that moved away from the boundary (to avoid absorption at short times) and are thus supposed to “forget” about their starting point. This behavior may sound even more puzzling after recalling the former study by Levitz *et al.*, in which the starting point was uniformly distributed near the absorbing boundary [19]. In this work, the persistence exponent  $\alpha$  was related via Eq. (2) to the fractal dimension  $d_f$  of the boundary. Can one claim that the power-law decay  $t^{-d_f/2}$  is an average of different power laws with  $\mathbf{x}_0$ -dependent persistence exponents over the starting point  $\mathbf{x}_0$ ? In the next subsection, we refine the analysis of the power-law decay in order to clarify this puzzling behavior.

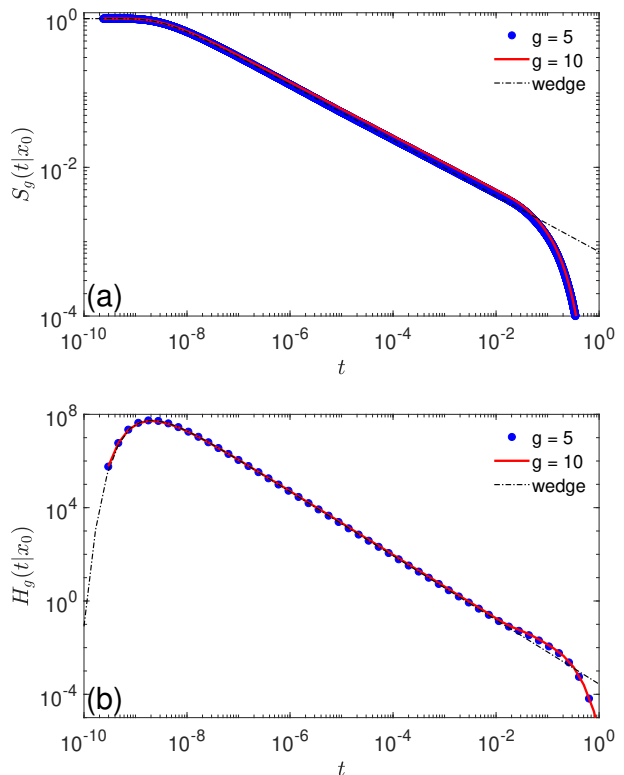


FIG. 8. (a) Survival probability  $S_g(t|\mathbf{x}_0)$  and (b) PDF  $H_g(t|\mathbf{x}_0)$  for two generations  $g = 5$  (circles) and  $g = 10$  (solid line) of the Koch snowflake, with  $\Theta = \pi/3$ ,  $L = 2$ ,  $D = 1$ ,  $r_0 = 10^{-4}$  and  $\theta_0 = \Theta/2$ , starting near the angle  $4\pi/3$  (Fig. 4(b)), obtained by Monte Carlo simulations with  $N = 10^8$  particles. Thin dash-dotted line shows the survival probability  $S_{4\pi/3,\infty}(t|\mathbf{x}_0)$  on panel (a) and the PDF  $H_{4\pi/3,\infty}(t|\mathbf{x}_0)$  on panel (b) for the wedge of angle  $4\pi/3$ , which decay as  $t^{-\alpha}$  and  $t^{-\alpha-1}$ , respectively, with  $\alpha = \pi/(2 \cdot 4\pi/3) = 0.375$ . Note that the exponential decay starts at  $t_c \approx 0.1$  given by Eq. (24).

## F. Local persistence exponent

The persistence exponent  $\alpha$  is usually estimated by fitting the survival probability to a power law. However, as the power-law behavior presents an intermediate regime in our setting, one needs to choose properly the range of timescales for fitting. As a consequence, the fitting procedure may be inaccurate and biased. To avoid these issues and to get a finer insight onto the asymptotic behavior of the survival probability, we introduce *the local persistence exponent* as the (negative) logarithmic derivative of  $S_g(t|\mathbf{x}_0)$ :

$$\alpha(t) = -\frac{d \ln S_g(t|\mathbf{x}_0)}{d \ln t}. \quad (29)$$

If the survival probability decayed as a power law with an exponent  $\alpha$  at all times, one would simply get  $\alpha(t) = \alpha$ . However, the actual behavior of the survival probability



is more sophisticated. At very short times, one has  $1 - S_g(t|\mathbf{x}_0) \propto e^{-h_0^2/(4Dt)}$ , where  $h_0$  is the distance to the boundary, so that  $\alpha(t) \rightarrow 0$  as  $t \rightarrow 0$ . At very long times, one has  $S_g(t|\mathbf{x}_0) \propto e^{-D\lambda_{\min}t}$  so that  $\alpha(t) \approx D\lambda_{\min}t \rightarrow +\infty$  because the exponential decay is faster than any power law. But if there was an intermediate power-law regime in between, one would get a plateau of  $\alpha(t)$  with a constant value that can be associated with the persistence exponent.

To evaluate the local persistence exponent numerically from a given empirical CDF, we define a range of  $K + 1$  times  $t_k = t_0(t_K/t_0)^{k/K}$  (with  $k = 0, 1, \dots, K$ ), which are equally spaced on the logarithmic scale between prescribed bounds  $t_0$  and  $t_K$ . By interpolating  $S_g(t_k|\mathbf{x}_0)$  from the empirical CDF, we set

$$\alpha(t'_k) = -\frac{\ln(S_g(t_k|\mathbf{x}_0)/S_g(t_{k-1}|\mathbf{x}_0))}{\ln(t_k/t_{k-1})} \quad (k = 1, \dots, K), \quad (30)$$

estimated at the intermediate time  $t'_k = \sqrt{t_k t_{k-1}}$  between  $t_{k-1}$  and  $t_k$  (the geometric mean is used to respect the logarithmic spacing of points). For  $K$  large enough, these values provide an accurate approximation for the logarithmic derivative. For the considered examples, we choose  $K = 100$ . We checked that the obtained results did not almost change when  $K$  was doubled. We also note that additional simulations with a minimal threshold  $T_{\min}$  were needed to get more accurate estimates of  $\alpha(t)$  at long times (see Sec. III B).

Figure 9 illustrates the local persistence exponents, which were obtained from the survival probabilities shown on Fig. 7(a), corresponding to the starting point near the vertex of angle  $\pi/3$  (Fig. 4(c)). Due to rarity of too small and too large FPTs, we could not access  $\alpha(t)$  accurately at very short and very long times so that we focused on the timespan between  $t_0 = 10^{-10}$  and  $t_K = 10^{-4}$ . As this figure conveys one of our main results, we discuss it in detail.

Let us first examine the local persistence exponent for the wedge of angle  $\Theta = \pi/3$  (dashed line). To get this curve, we first computed the survival probability  $S_{\Theta, \infty}(t|\mathbf{x}_0)$  from Eq. (15) at numerous time instances, recasted it as an empirical CDF, and then applied the above numerical procedure. Expectedly,  $\alpha(t)$  starts from 0 at  $t \rightarrow 0$  and then grows monotonically to reach a plateau for  $t \gtrsim 10^{-7}$ . This plateau corresponds to the persistence exponent  $\alpha = \pi/(2\Theta) = 3/2$  of the wedge. Next, we look at  $\alpha(t)$  for the generation  $g = 5$  (triangles). As the survival probability  $S_5(t|\mathbf{x}_0)$  was very close to  $S_{\Theta, \infty}(t|\mathbf{x}_0)$  up to  $t \approx 4 \cdot 10^{-6}$  (Fig. 7(a)), their local persistence exponents are almost identical over this time range. However, at longer times,  $\alpha(t)$  starts to deviate from the plateau. This timescale determines a typical diffusion length  $\sqrt{4Dt} \approx 4 \cdot 10^{-3}$ , which is comparable to the length  $\ell_5 \approx 8.2 \cdot 10^{-3}$  of the segments. In other words, at times  $t \gtrsim 4 \cdot 10^{-6}$ , the particle starts to “feel” that the absorbing boundary is not a wedge but the 5-th generation of the Koch snowflake, and thus the survival

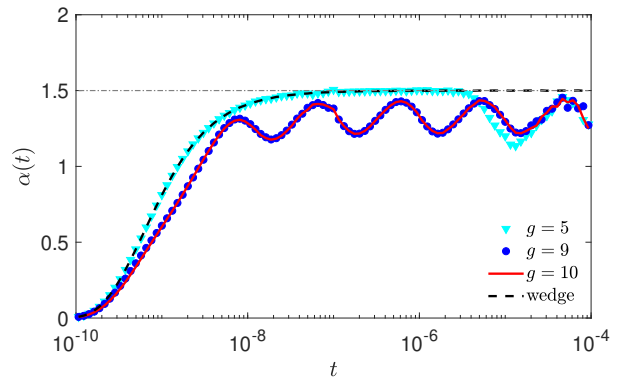


FIG. 9. Local persistence exponent  $\alpha(t)$  for three generations  $g = 5$  (triangles),  $g = 9$  (circles) and  $g = 10$  (solid line) of the Koch snowflake, with  $\Theta = \pi/3$ ,  $L = 2$ ,  $D = 1$ ,  $r_0 = 10^{-4}$  and  $\theta_0 = \Theta/2$ , starting near the angle  $\pi/3$  (Fig. 4(c)), obtained by Monte Carlo simulations with  $N = 10^8$  particles (its behavior for  $t > T_{\min} = 10^{-7}$  was estimated from additional simulations, see Sec. III B). Dashed line presents the local persistence exponent for the wedge of angle  $\pi/3$ , whereas dash-dotted horizontal line indicates its persistence exponent  $3/2$  (in the limit  $t \rightarrow \infty$ ).

probability  $S_g(t|\mathbf{x}_0)$  deviates from  $S_{\Theta, \infty}(t|\mathbf{x}_0)$ .

The most striking behavior is observed for generations  $g = 9$  and  $g = 10$ . After a short transient regime of growing  $\alpha(t)$ , the local persistence exponent starts to oscillate (on the logarithmic scale), still remaining below  $3/2$ . Since the curves for generations  $g = 9$  and  $g = 10$  are almost identical, we can claim that this behavior is independent of the generation (if  $g$  is not small) and thus representative of the behavior in the limit  $g \rightarrow \infty$ , i.e., to the fractal boundary. The earlier reported value of the persistence exponent from fitting a power law, 1.25, is the average level of oscillations. Note that the local persistence exponent for the generation  $g = 5$  also approaches these log-periodic oscillations at times  $t \gtrsim 4 \cdot 10^{-6}$ . This numerical observation conveys that the survival probability in the Koch snowflake does not exhibit a power-law decay and thus cannot be characterized by a persistence exponent. In turn, the local persistence exponent reveals much finer details of the asymptotic behavior and its relation to the geometric structure of the fractal boundary.

How many log-periodic oscillations of  $\alpha(t)$  can exist? Figure 9 revealed five log-periodic oscillations on the considered timespan from  $10^{-10}$  to  $10^{-4}$ . Extending this pattern hypothetically to longer times, several additional oscillations can be expected, up to the exponential cut-off  $t_c \approx 10^{-1}$ , above which  $\alpha(t)$  should exhibit a linear growth with  $t$ . In other words, the cut-off time  $t_c$  sets the upper bound on the time range of log-periodic oscillations. In turn, the lower bound is determined by the transient growth of  $\alpha(t)$  at short times, which is controlled by the initial distance to the boundary. If one could generate a sufficiently accurate statistics of the FPT at arbitrarily

small distance  $h_0$  from the boundary  $\partial\Omega_g$  of arbitrary high generation  $g$ , the log-periodic pattern of  $\alpha(t)$  could be extended to the left to arbitrarily short times.

The observed log-periodic oscillations reflect self-similarity of the Koch boundary. Indeed, if  $T_1, T_2, \dots$  denote the time instances of the successive maxima of  $\alpha(t)$ , we observe  $T_{k+1}/T_k \approx 9$ , whereas the ratio of the associated length scales,  $\sqrt{DT_{k+1}}/\sqrt{DT_k}$ , is around 3. This is precisely the scaling factor between two successive generations of the Koch boundary with  $\Theta = \pi/3$ . This simple relation suggests the following interpretation.

Let us look at the local geometric environment near the starting point indicated by a gray zone in Fig. 10(a). Most particles are absorbed by the boundary in a close vicinity of the starting point, within a distance  $h$ , which is comparable to the distance  $h_0$  to the boundary, yielding the most probable FPT of the order of  $h^2/(6D)$ . As a consequence, the short-time behavior of the survival probability is mostly determined by this local environment. Moreover, since the local persistence exponents for generations  $g = 9$  and  $g = 10$  on Fig. 9 were almost identical, the inclusion of the smaller geometric details at the iteration from  $g = 9$  to  $g = 10$  does not seem to affect the first-passage times. This is consistent with the fact that most trajectories are stopped at the most accessible parts of the boundary (see [25, 26] for the related discussion on the harmonic measure). In turn, the survival probability at longer times describes the trajectories that managed to avoid hitting this local environment and thus reached a larger gray zone shown in Fig. 10(b). Qualitatively, such trajectories can be treated as if they just started from a random point inside the larger gray zone. The self-similar structure of the boundary allows one to repeat this argument again and again so that the survival of the particle at longer and longer times can be understood as a sequence of successful “escapes” from one zone to the larger one. This sequence is repeated until the particle arrives into central part of the Koch snowflake where it starts to “feel” the confinement and thus switches to the exponential decay. As a consequence, the log-periodic pattern in the local persistence exponent  $\alpha(t)$  reflects the self-similarity of the absorbing boundary. Qualitatively, the number of oscillations should thus be equal to the number of “escapes”, which is a purely geometric characteristic that depends on the starting point.

After this qualitative argument, it is instructive to revisit the survival probability shown on Fig. 8(a) for another starting point near the angle  $4\pi/3$ . Figure 11 shows that the local persistence exponents for generations  $g = 5$  and  $g = 10$  are almost identical and are actually close to that of the wedge of angle  $4\pi/3$ . At long times, the latter reaches the limit  $3/8$ , i.e., the persistence exponent for the wedge. In this setting, the diffusing particle is either rapidly absorbed in the local environment of its starting point (which is close to that of a wedge), or easily reaches the central part of the Koch snowflake, with almost no effect of the self-similar boundary. In other words, there is

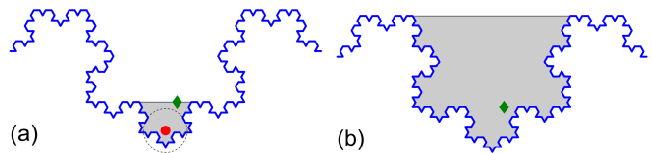


FIG. 10. **(a)** Local environment around the starting point (red circle) located near the boundary of the Koch snowflake with  $\Theta = \pi/3$  (a small fraction of the boundary is shown). Dashed circle of radius  $h$  indicates a close vicinity of the boundary, on which most particles are rapidly absorbed.

To avoid rapid absorption, the particle needs to leave the gray zone, e.g., through a randomly chosen point indicated by green diamond. **(b)** To avoid absorption at a longer time, the particle at green diamond needs to leave a new gray zone, which is three times bigger than the previous one.

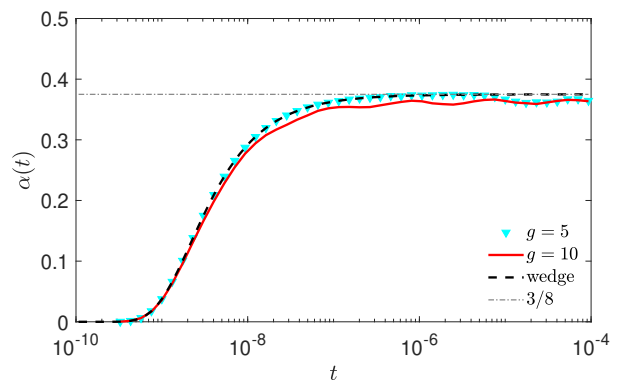


FIG. 11. Local persistence exponent  $\alpha(t)$  for two generations  $g = 5$  (triangles) and  $g = 10$  (solid line) of the Koch snowflake, with  $\Theta = \pi/3$ ,  $L = 2$ ,  $D = 1$ ,  $r_0 = 10^{-4}$  and  $\theta_0 = 2\pi/3$ , starting near the angle  $4\pi/3$  (Fig. 4(b)), obtained by Monte Carlo simulations with  $N = 10^8$  particles. Dashed line shows the local persistence exponent of the survival probability  $S_{4\pi/3, \infty}(t|\mathbf{x}_0)$  of the wedge of angle  $4\pi/3$ , while dash-dotted horizontal line indicates its long-time asymptotic value  $3/8$ .

no a sequence of “escapes” from smaller to larger zones, and the local persistence exponent  $\alpha(t)$  remains almost constant (and close to the value  $3/8$  for the wedge).

Finally, we revisit the asymptotic behavior of the survival probability  $S_g(t)$  in the case when the starting point is uniformly distributed near the boundary. As discussed earlier, this survival probability exhibits a power-law decay (2) with the persistence exponent  $\alpha = d_f/2$  [19]. Figure 12 shows the local persistence exponent in this case for generations from  $g = 5$  to  $g = 10$ . For  $g = 10$ , we get small oscillations around  $\alpha = d_f/2 \approx 0.63$ . Since the chosen distance  $h_0 = 10^{-5}$  to the boundary is smaller than the segment length  $\ell_{10} \approx 3.39 \cdot 10^{-5}$ , we do not see a transient regime, which should be present at much smaller times. For  $g = 5$ , one has  $h_0 \ll \ell_5 \approx 8.2 \cdot 10^{-3}$  so that the particle first explores a flat local environment,

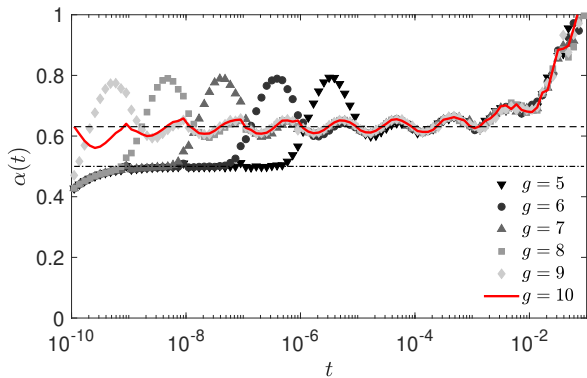


FIG. 12. Local persistence exponent  $\alpha(t)$  for six generations from  $g = 5$  (light diamonds) to  $g = 10$  (solid line) of the Koch snowflake, with  $\Theta = \pi/3$ ,  $L = 2$ ,  $D = 1$ , and the uniformly distributed starting point at distance  $h_0 = 10^{-5}$  from the boundary, obtained by Monte Carlo simulations with  $N = 10^8$  particles (an extended simulation for  $t > T_{\min} = 10^{-6}$  with  $N_0 = 10^7$  was also included, see Sec. III B). Dashed horizontal line indicates the persistence exponent  $d_f/2 \approx 0.63$ , while dash-dotted line presents the persistence exponent  $1/2$  of a flat boundary.

and the local persistence exponent is close to  $1/2$  at short times. In turn, one observes a transition to  $\alpha \approx 0.63$  at longer times. As the generation  $g$  increases,  $\ell_g$  gets smaller and smaller, so that the transition to  $\alpha \approx 0.63$  occurs at shorter and shorter times. For all considered generations, we also observe a growth of  $\alpha(t)$  at times  $t$  larger than  $10^{-2}$ , as expected at very long times. This observation was possible because the survival probability  $S_g(t)$  decays slower than  $S_g(t|\mathbf{x}_0)$  considered earlier, so that our Monte Carlo simulations were accurate enough to estimate  $S_g(t)$  over a broader timespan.

#### IV. DISCUSSION AND CONCLUSION

In this paper, we studied the distribution of the FPT to the absorbing self-similar boundary of the Koch snowflake. An accurate examination of this problem in a circular sector and a wedge allowed us to outline three distinct regimes at short, intermediate, and long times. The first and the third regimes characterize respectively too short and too long trajectories and exhibit universal, well-known features. In turn, the intermediate regime is geometry-dependent and less understood in general. When the starting point is fixed and located near a smooth absorbing boundary, the intermediate regime exhibits a power-law decay with the persistence exponent  $\alpha = 1/2$ , inherited from the Lévy-Smirnov distribution on the half-line. For irregular boundaries, however, the persistence exponent is controlled by singularities (e.g.,  $\alpha = \pi/(2\Theta)$  for a wedge of angle  $\Theta$ ). If there are many different angles, their effect onto the distribution of the

FPT can be more sophisticated. One can expect that the angle that is the nearest to the starting point would affect the survival probability first, at time scales of the order  $r_0^2/D$ , where  $r_0$  is the distance to that angle. However, at longer times, the survived random trajectories can explore more distant regions and thus be affected by farther angles. This intuitive picture gives an idea that the decay of the survival probability is not necessarily controlled by a single persistence exponent but may exhibit distinct decay laws at different time scales. In other words, a single power law may be insufficient to fully characterize the survival of a particle in complex domains.

Our extensive Monte Carlo simulations confirmed this intuitive picture. For this purpose, we introduced the local persistence exponent  $\alpha(t)$  as the logarithmic derivative of the survival probability, i.e.,  $S(t) \propto t^{-\alpha(t)}$ . As this relation can formally be applied to any positive function  $S(t)$ , the local persistence exponent  $\alpha(t)$  is just a convenient representation of the survival probability. In particular, if  $\alpha(t)$  varies with time, the survival probability does not obey a power law. Our numerical results revealed four possible regimes for  $\alpha(t)$ : (i)  $\alpha(t) \rightarrow 0$  as  $t \rightarrow 0$  in agreement with the Lévy-Smirnov short-time behavior of the survival probability; in particular, there is a transient growth of  $\alpha(t)$  at short times; (ii)  $\alpha(t) \approx 1/2$  or  $\alpha(t) \approx \pi/(2\Theta)$  at early intermediate times when  $h_0 \ll \ell_g$ , i.e., if the particle started close to a linear segment of length  $\ell_g$  of the polygonal boundary  $\partial\Omega_g$  (the  $g$ -th generation of the Koch snowflake); (iii)  $\alpha(t)$  exhibits log-periodic oscillations at late intermediate times; and (iv)  $\alpha(t) \propto t$  at long times due to the exponential decay of the survival probability in a bounded domain. While the first and the last regimes are universal and always present for any bounded domain, the two intermediate regimes strongly depend on the considered domain and the starting point. For instance, in the case of finite generations of the Koch snowflake, we gave examples when both regimes are present (curve for  $g = 5$  on Fig. 9), only the second regime is present (Fig. 11), only the third regime is present (curve for  $g = 10$  on Fig. 9).

The log-periodic oscillations of the local persistence exponent of the survival probability present the main finding of the paper. The self-similarity of the absorbing boundary was identified as their origin. Indeed, the survival at longer and longer times requires moving away from the absorbing boundary, as far as possible, into the bulk. The repeated pattern of  $\alpha(t)$  results from a sequence of successive “escapes” into larger and larger regions, which are rescaled copies of each other. The number of log-periodic oscillations reflects how many such successively enlarged regions are present on the path from the starting point to the central part of the Koch snowflake. In particular, in the case of the infinite generation of the fractal boundary, one should be able to get any number of log-periodic oscillations by locating the starting point arbitrarily close to the boundary. In other words, the oscillatory behavior of  $\alpha(t)$  can cover an

arbitrarily broad timespan. In this regime, the survival probability does not exhibit a power-law decay and thus cannot be characterized by a single persistence exponent. This important feature of the diffusive dynamics seems to be overseen in the past, possibly because most earlier works were focused either on a uniform starting point, or on the MFPT. Fixing the starting point near the absorbing boundary allowed us to uncover new and richer aspects of this phenomenon.

This numerical discovery raises many fundamental questions. While log-periodicity of  $\alpha(t)$  can be explained by self-similarity, the shape of its motive remains unclear. As the diffusing particle aims to escape from the local polygonal environment formed by a mixture of different angles (here,  $\pi/3$  and  $4\pi/3$ ), one can speculate that the shape of one period in  $\alpha(t)$  results from averaging between distinct power laws over a limited timespan. It would be interesting to relate the shape of the periodic pattern to the geometric structure of the local environment. Moreover, one can also determine how the average  $\alpha(t)$  and the amplitude of its oscillations depend on the geometry (e.g., on the angle  $\Theta$  of the generator of the Koch snowflake or, more generally, on the fractal dimension). Another question concerns the analysis of more sophisticated fractal boundaries. In fact, even though fractal boundaries often emerge in natural applications [68–71], their self-similarity is generally not perfect, and one often deals with heterogeneous structures, multifractals, or random fractals. For instance, one can still consider the iterative construction of the Koch snowflake but choose randomly the orientation of the generator. In this way, one would produce a random fractal with the same fractal dimension  $d_f$  given by Eq. (22). The earlier numerical work by Filoche and Sapoval showed that the steady-state diffusive fluxes towards random and deterministic fractals with the same  $d_f$  are essentially identical, i.e., randomness is not so relevant [72]. What would be the impact of randomness or heterogeneity onto the asymptotic behavior of the survival probability? Another interesting perspective consists in extending the above analysis to exterior problems (i.e., diffusion outside a target with a fractal boundary) and to higher dimensions.

Finally, the survival probability in any bounded domain admits a spectral decomposition over the eigenvalues  $\lambda_n$  and eigenfunctions  $u_n(\mathbf{x})$  of the Dirichlet Laplace

operator in that domain:

$$S(t|\mathbf{x}_0) = \sum_{n=1}^{\infty} e^{-Dt\lambda_n} u_n(\mathbf{x}_0) \int_{\Omega} d\mathbf{x} u_n(\mathbf{x}). \quad (31)$$

The log-periodic pattern of the local persistence exponent of  $S(t|\mathbf{x}_0)$  should thus be related to the geometrical structure of these eigenmodes, which often exhibit self-similar features [51, 62–66]. A similar relation between the log-periodic behavior of the heat kernel and the spectrum of the Laplace operator was investigated for *fractal domains* (see [73] and references therein). In particular, the MFPT in such domains was shown to exhibit spatial log-periodic oscillations [74]. More generally, log-periodic oscillations were observed in various physical systems exhibiting discrete scale invariance, with examples ranging from critical phenomena and chaotic dynamics to turbulence and financial crashes [75–77]. As explained in Sec. I, our setting of ordinary diffusion in a Euclidean domain with a *fractal boundary* is drastically different and, perhaps, more challenging for mathematical analysis. For instance, the fractal boundary is known to affect only the subleading term of the heat trace and the Weyl’s law [78–80] (see also [81] for random walks on Vicsek fractals), i.e., it requires finer mathematical tools. In particular, we saw the strong dependence of the asymptotic behavior on the starting point. Further clarifications of the fundamental relation between log-periodic oscillations of the survival probability and the Laplacian spectrum presents an important perspective of this study.

## ACKNOWLEDGMENTS

The authors thank Prof. M. Dolgushev for reading the manuscript and fruitful discussions. D.S.G. acknowledges the Simons Foundation for supporting his sabbatical sojourn in 2024 at the CRM (University of Montréal, Canada), as well as the Alexander von Humboldt Foundation for support within a Bessel Prize award.

## Appendix A: Computation of the second moment

Using the spectral representation (6), one can evaluate the second moment of the FPT in the sector:

$$\begin{aligned}
T_{\Theta,R}^{(2)} &= \int_0^\infty dt t^2 H_{\Theta,R}(t|\mathbf{x}_0) = 2 \int_0^\infty dt t S_{\Theta,R}(t|\mathbf{x}_0) \\
&= \frac{8}{\Theta} \sum_{n=1}^\infty \sum_{k=1}^\infty \frac{c_{nk}^2}{D^2 \lambda_{nk}^2} \sin(\nu_n \theta_0) J_{\nu_n}(\alpha_{nk} r_0/R) \frac{1 - (-1)^n}{\nu_n} R^2 \int_0^1 dx x J_{\nu_n}(\alpha_{nk} x) \\
&= \frac{8R^4}{\Theta D^2} \sum_{n=1}^\infty \frac{1 - (-1)^n}{\nu_n} \sin(\nu_n \theta_0) \int_0^1 dx x \sum_{k=1}^\infty \frac{J_{\nu_n}(\alpha_{nk} r_0/R) J_{\nu_n}(\alpha_{nk} x)}{\alpha_{nk}^4 J_{\nu_n+1}^2(\alpha_{nk})}.
\end{aligned}$$

In order to compute the last sum, we use the summation identity (see (D10) from Table 3 in [53]):

$$\begin{aligned}
&\sum_{k=1}^\infty \frac{2J_{\nu_n}(\alpha_{nk} x_0) J_{\nu_n}(\alpha_{nk} x)}{(z^2 - \alpha_{nk}^2) J_{\nu_n+1}^2(\alpha_{nk})} \\
&= \frac{\pi}{2} \left( Y_{\nu_n}(zx_0) - J_{\nu_n}(zx_0) \frac{Y_{\nu_n}(z)}{J_{\nu_n}(z)} \right) J_{\nu_n}(zx), \quad (\text{A1})
\end{aligned}$$

which is valid for  $0 \leq x \leq x_0 \leq 1$  (note that the factor  $\pi/2$  was missing in Eq. (D10)). Evaluating the derivative with respect to  $z$ , dividing by  $z$  and taking the limit  $z \rightarrow 0$ , we get for  $0 \leq x \leq x_0 \leq 1$

$$\begin{aligned}
&\sum_{k=1}^\infty \frac{J_{\nu_n}(\alpha_{nk} x_0) J_{\nu_n}(\alpha_{nk} x)}{\alpha_{nk}^4 J_{\nu_n+1}^2(\alpha_{nk})} = \frac{x^{\nu_n}}{16\nu_n(\nu_n+1)x_0^{\nu_n}} \\
&\times \left( x_0^2(x_0^{2\nu_n} - (1+a_{\nu_n})x_0^{2\nu_n-2} + a_{\nu_n}) - x^2(1-x_0^{2\nu_n}) \right), \quad (\text{A2})
\end{aligned}$$

where  $a_\nu = (\nu+1)/(\nu-1)$ . Substituting this expression into the above formula for the second moment, we get after simplifications

$$T_{\Theta,R}^{(2)} = \frac{R^4}{\Theta D^2} \sum_{n=1}^\infty \frac{1 - (-1)^n}{\nu_n(\nu_n+1)} \sin(\nu_n \theta_0) f_{\nu_n}(r_0/R), \quad (\text{A3})$$

where

$$\begin{aligned}
f_\nu(x_0) &= \frac{4(\nu+1)}{(\nu^2-4)(\nu^2-16)} x_0^4 \\
&\quad - \frac{\nu+6}{(\nu+2)(\nu^2-16)} x_0^\nu + \frac{1}{\nu^2-4} x_0^{\nu+2}. \quad (\text{A4})
\end{aligned}$$

Note that the sum involving the first term in Eq. (A4) can be evaluated exactly that yields

$$\begin{aligned}
T_{\Theta,R}^{(2)} &= T_{\Theta,\infty}^{(2)} + \frac{R^4}{\Theta D^2} \sum_{n=1}^\infty \frac{1 - (-1)^n}{\nu_n(\nu_n+1)} \sin(\nu_n \theta_0) \\
&\quad \times \left( -\frac{(\nu_n+6)(r_0/R)^{\nu_n}}{(\nu_n+2)(\nu_n^2-16)} + \frac{(r_0/R)^{\nu_n+2}}{\nu_n^2-4} \right), \quad (\text{A5})
\end{aligned}$$

where

$$T_{\Theta,\infty}^{(2)} = \frac{r_0^4}{96D^2} \left( \frac{\cos(4\theta_0 - 2\Theta)}{\cos(2\Theta)} - 4 \frac{\cos(2\theta_0 - \Theta)}{\cos(\Theta)} + 3 \right). \quad (\text{A6})$$

Combining this result with Eq. (12) for the first moment, we get the standard deviation of the FPT,

$$\delta T_{\Theta,R} = \sqrt{T_{\Theta,R}^{(2)} - (T_{\Theta,R})^2}. \quad (\text{A7})$$

In order to determine the leading order in the asymptotic behavior of the second moment as  $r_0 \rightarrow 0$ , we distinguish two cases. When  $\Theta > \pi/4$ , one has  $\nu_1 = \pi/\Theta < 4$ , so that the leading-order contribution comes from the term  $n=1$  of the series in Eq. (A5) that scales as

$$\frac{D^2}{R^4} T_{\Theta,R}^{(2)} \approx \frac{2(\nu_1+6) \sin(\nu_1 \theta_0)}{\pi(\nu_1+1)(\nu_1+2)(16-\nu_1^2)} (r_0/R)^{\pi/\Theta}. \quad (\text{A8})$$

In turn, if  $\Theta < \pi/4$ , the leading contribution is given by  $T_{\Theta,\infty}^{(2)}$  from Eq. (A6), which scales as  $r_0^4$ . Combining these relations with Eqs. (14) for the first moment, we deduce the asymptotic behavior of the standard deviation:

$$\frac{D}{R^2} \delta T_{\Theta,R} \approx \begin{cases} \sqrt{\frac{2(\nu_1 + 6) \sin(\nu_1 \theta_0)}{\pi(\nu_1 + 1)(\nu_1 + 2)(16 - \nu_1^2)}} (r_0/R)^{\pi/(2\Theta)} & (\Theta > \pi/4), \\ \frac{1}{\sqrt{96}} \left( \frac{\cos(4\theta_0 - 2\Theta)}{\cos(2\Theta)} - 6 \frac{\cos^2(2\theta_0 - \Theta)}{\cos^2(\Theta)} + 8 \frac{\cos(2\theta_0 - \Theta)}{\cos(\Theta)} - 3 \right)^{1/2} (r_0/R)^2 & (\Theta < \pi/4). \end{cases} \quad (\text{A9})$$

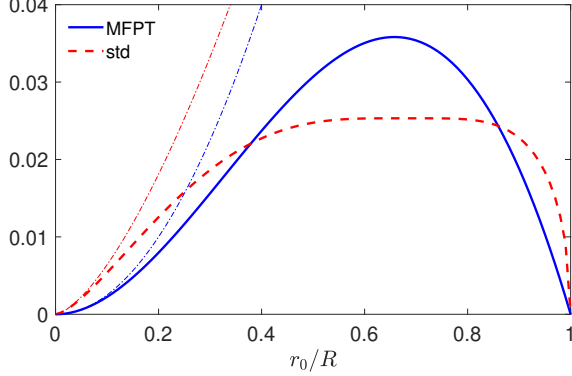


FIG. 13. MFPT (solid line) and the standard deviation of the FPT (dashed line) as functions of the distance  $r_0$  to the origin of the sector  $\Omega_{\Theta,R}$ , with  $\Theta = \pi/3$  and  $R = 1$ . Thin dash-dotted lines present the asymptotic relations (14, A9).

One can thus distinguish three regimes:

$$\frac{\delta T_{\Theta,R}}{T_{\Theta,R}} \propto \begin{cases} 1 & (0 < \Theta < \pi/4), \\ (r_0/R)^{\pi/(2\Theta)-2} & (\pi/4 < \Theta < \pi/2), \\ (r_0/R)^{-\pi/(2\Theta)} & (\pi/2 < \Theta). \end{cases} \quad (\text{A10})$$

In particular, one sees that the relative standard deviation diverges as  $r_0 \rightarrow 0$  for  $\Theta > \pi/4$ .

Figure 13 illustrates the behavior of the MFPT and the standard deviation of the FPT for the sector with  $\Theta = \pi/3$ . When the starting point is far from the boundary ( $r_0/R \sim 0.5$ ), the standard deviation is comparable to the MFPT that is a common situation for diffusive search in a bounded domain. In turn, as  $r_0 \rightarrow 0$ , both MFPT and the standard deviation tend to 0, but the MFPT vanishes much faster. As a consequence, the standard deviation is much bigger than the MFPT, while their ratio diverges according to Eq. (A10).

- 
- [1] S. Redner, *A Guide to First Passage Processes* (Cambridge: Cambridge University press, 2001).
- [2] R. Metzler, G. Oshanin, and S. Redner (Eds.) *First-Passage Phenomena and Their Applications* (Singapore: World Scientific, 2014).
- [3] J. Masoliver, *Random Processes: First-passage And Escape* (World Scientific Publishing, 2018).
- [4] G. Oshanin, R. Metzler, K. Lindenberg (Eds.) *Chemical Kinetics: Beyond the Textbook* (New Jersey: World Scientific, 2019).
- [5] L. Dagdug, J. Peña and I. Pompa-García, *Diffusion Under Confinement. A Journey Through Counterintuition* (Springer, 2024).
- [6] B. Meyer, C. Chevalier, R. Voituriez, and O. Bénichou, Universality classes of first-passage-time distribution in confined media, *Phys. Rev. E* **83**, 051116 (2011).
- [7] A. Singer, Z. Schuss, D. Holcman, and R. S. Eisenberg, Narrow Escape, Part I, *J. Stat. Phys.* **122**, 437 (2006).
- [8] S. Condamin, O. Bénichou, and M. Moreau, Random walks and Brownian motion: A method of computation for first-passage times and related quantities in confined geometries, *Phys. Rev. E* **75**, 021111 (2007).
- [9] O. Bénichou, B. Meyer, V. Tejedor, and R. Voituriez, Zero Constant Formula for First-Passage Observables in Bounded Domains, *Phys. Rev. Lett.* **101**, 130601 (2008).
- [10] E. Agliari, Exact mean first-passage time on the T-graph, *Phys. Rev. E* **77**, 011128 (2008).
- [11] S. Pillay, M. J. Ward, A. Peirce, and T. Kolokolnikov, An Asymptotic Analysis of the Mean First Passage Time for Narrow Escape Problems. Part I. Two-Dimensional Domains, *SIAM Multi Model. Simul.* **8**, 803 (2010).
- [12] T. G. Mattos, C. Mejia-Monasterio, R. Metzler, and G. Oshanin, First passages in bounded domains: When is the mean first passage time meaningful?, *Phys. Rev. E* **86**, 031143 (2012).
- [13] O. Bénichou and R. Voituriez, From first-passage times of random walks in confinement to geometry-controlled kinetics, *Phys. Rep.* **539**, 225-284 (2014).
- [14] D. Holcman and Z. Schuss, The Narrow Escape Problem, *SIAM Rev.* **56**, 213-257 (2014).
- [15] O. Bénichou, T. Guérin, and R. Voituriez, Mean first-passage times in confined media: from Markovian to non-Markovian processes, *J. Phys. A: Math. Theor.* **48**, 163001 (2015).
- [16] D. S. Grebenkov, Universal formula for the mean first passage time in planar domains, *Phys. Rev. Lett.* **117**, 260201 (2016).
- [17] M. J. Simpson, D. J. VandenHeuvel, J. M. Wilson, S. W. McCue, and E. J. Carr, Mean exit time for diffusion on irregular domains, *New J. Phys.* **23**, 043030 (2021).
- [18] A. J. Bray, S. N. Majumdar, and G. Schehr, Persistence and First-Passage Properties in Non-equilibrium Systems, *Adv. Phys.* **62**, 225-361 (2013).
- [19] P. Levitz, D. S. Grebenkov, M. Zinsmeister, K. M. Kolwankar, and B. Sapoval, Brownian flights over a fractal nest and first passage statistics on irregular surfaces, *Phys. Rev. Lett.* **96**, 180601 (2006).
- [20] A. Rozanova-Pierrat, D. S. Grebenkov, and B. Sapoval,

- Faster Diffusion across an Irregular Boundary, *Phys. Rev. Lett.* **108**, 240602 (2012).
- [21] M. E. Cates and T. A. Witten, Diffusion near absorbing fractals: Harmonic measure exponents for polymers, *Phys. Rev. A* **35**, 1809 (1987).
- [22] B. B. Mandelbrot and C. J. G. Evertsz, The potential distribution around growing fractal clusters, *Nature* **348**, 143 (1990).
- [23] C. J. G. Evertsz, P. W. Jones, and B. B. Mandelbrot, Behaviour of the harmonic measure at the bottom of fjords, *J. Phys. A: Math. Gen.* **24**, 1889 (1991).
- [24] C. J. G. Evertsz and B. B. Mandelbrot, Harmonic measure around a linearly self-similar tree, *J. Phys. A: Math. Gen.* **25**, 1781 (1992).
- [25] D. S. Grebenkov, A. A. Lebedev, M. Filoche, and B. Sapoval, Multifractal Properties of the Harmonic Measure on Koch Boundaries in Two and Three Dimensions, *Phys. Rev. E* **71**, 056121 (2005).
- [26] D. S. Grebenkov, What Makes a Boundary Less Accessible, *Phys. Rev. Lett.* **95**, 200602 (2005).
- [27] D. A. Adams, L. M. Sander, E. Somfai, and R. M. Ziff, The harmonic measure of diffusion-limited aggregates including rare events, *EPL* **87**, 20001 (2009).
- [28] T. A. Witten and L. M. Sander, Diffusion-Limited Aggregation, a Kinetic Critical Phenomenon, *Phys. Rev. Lett.* **47**, 1400 (1981).
- [29] T. C. Halsey, Diffusion-limited aggregation as branched growth, *Phys. Rev. Lett.* **72**, 1228 (1994).
- [30] D. S. Grebenkov and D. Beliaev, How anisotropy beats fractality in two-dimensional on-lattice DLA growth, *Phys. Rev. E* **96**, 042159 (2017).
- [31] D. Stauffer and A. Aharony, *Introduction to Percolation Theory* (Taylor & Francis, 1992).
- [32] B. O'Shaughnessy and I. Procaccia, Analytical solutions for diffusion on fractal objects, *Phys. Rev. Lett.* **54**, 455-458 (1985).
- [33] C. Van den Broeck, Renormalization of first-passage times for random walks on deterministic fractals, *Phys. Rev. A* **40**, 7334 (1989).
- [34] S. Condamin, O. Bénichou, V. Tejedor, R. Voituriez, and J. Klafter, First-passage time in complex scale-invariant media, *Nature* **450**, 77 (2007).
- [35] S. Condamin, V. Tejedor, R. Voituriez, O. Bénichou, and J. Klafter, Probing microscopic origins of confined subdiffusion by first-passage observables, *Proc. Natl. Acad. Sci. U.S.A.* **105**, 5675-5680 (2008).
- [36] C. P. Haynes and A. P. Roberts, Global first-passage times of fractal lattices, *Phys. Rev. E* **78**, 041111 (2008).
- [37] O. Bénichou, C. Chevalier, J. Klafter, B. Meyer, and R. Voituriez, Geometry-controlled kinetics, *Nat. Chem.* **2**, 472-477 (2010).
- [38] Y. Lin, B. Wu, and Z. Zhang, Determining mean first-passage time on a class of treelike regular fractals, *Phys. Rev. E* **82**, 031140 (2010).
- [39] Y. Meroz, I. M. Sokolov, and J. Klafter, Distribution of first-passage times to specific targets on compactly explored fractal structures, *Phys. Rev. E* **83**, 020104(R) (2011).
- [40] B. Meyer, E. Agliari, O. Bénichou, and R. Voituriez, Exact calculations of first-passage quantities on recursive networks, *Phys. Rev. E* **85**, 026113 (2012).
- [41] F. Tavani and E. Agliari, First-passage phenomena in hierarchical networks, *Phys. Rev. E* **93**, 022133 (2016).
- [42] D. Plyukhin and A. V. Plyukhin, Random walks with fractally correlated traps: Stretched exponential and power-law survival kinetics, *Phys. Rev. E* **94**, 042132 (2016).
- [43] J. Peng and E. Agliari, First encounters on combs, *Phys. Rev. E* **100**, 062310 (2019).
- [44] N. Levernier, M. Dolgushev, O. Bénichou, R. Voituriez, and T. Guérin, Survival probability of stochastic processes beyond persistence exponents, *Nat. Commun.* **10**, 2990 (2019).
- [45] J. D. Hyman, M. Dentz, A. Hagberg, and P. K. Kang, Emergence of stable laws for first passage times in three-dimensional random fracture networks, *Phys. Rev. Lett.* **123**, 248501 (2019).
- [46] C. Zunke, J. Bewerunge, F. Platten, S. U. Egelhaaf, and A. Godec, First-passage statistics of colloids on fractals: Theory and experimental realization, *Sci. Adv.* **8**, eabk0627 (2022).
- [47] T. Baravi and E. Barkai, First passage times in compact domains exhibits bi-scaling (preprint ArXiv:2311.13915, 2023).
- [48] G. Lamé, *Leçons sur la Théorie Mathématique de l'Elasticité des Corps Solides* (Bachelier, Paris, 1852).
- [49] M. A. Pinsky, The Eigenvalues of an Equilateral Triangle, *SIAM J. Math. Anal.* **11**, 819 (1980).
- [50] M. A. Pinsky, Completeness of the Eigenfunctions of the Equilateral Triangle, *SIAM J. Math. Anal.* **16**, 848 (1985).
- [51] D. S. Grebenkov and B.-T. Nguyen, Geometrical structure of Laplacian eigenfunctions, *SIAM Rev.* **55**, 601-667 (2013).
- [52] G. N. Watson, *A Treatise on the Theory of Bessel Functions* (Cambridge University Press, Cambridge, 1962).
- [53] D. S. Grebenkov, A physicist's guide to explicit summation formulas involving zeros of Bessel functions and related spectral sums, *Rev. Math. Phys.* **33**, 2130002 (2021).
- [54] F. Le Vot, S. B. Yuste, E. Abad, and D. S. Grebenkov, First-encounter time of two diffusing particles in confinement, *Phys. Rev. E* **102**, 032118 (2020).
- [55] D. Considine and S. Redner, Repulsion of random and self-avoiding walks from excluded points and lines, *J. Phys. A: Math. Gen.* **22**, 1621-1638 (1989).
- [56] A. Comtet and J. Desbois, Brownian motion in wedges, last passage time and the second arc-sine law, *J. Phys. A: Math. Gen.* **36**, L255 (2003).
- [57] M. Chupeau, O. Bénichou, and S. N. Majumdar, Survival probability of a Brownian motion in a planar wedge of arbitrary angle, *Phys. Rev. E* **91**, 032106 (2015).
- [58] D. L. L. Dy and J. P. Esguerra, First-passage-time distribution for diffusion through a planar wedge, *Phys. Rev. E* **78**, 062101 (2008).
- [59] D. L. L. Dy and J. P. Esguerra, First-passage characteristics of biased diffusion in a planar wedge, *Phys. Rev. E* **88**, 012121 (2013).
- [60] A. Godec and R. Metzler, Universal proximity effect in target search kinetics in the few-encounter limit, *Phys. Rev. X* **6**, 041037 (2016).
- [61] D. S. Grebenkov, R. Metzler, and G. Oshanin, Strong defocusing of molecular reaction times results from an interplay of geometry and reaction control, *Commun. Chem.* **1**, 96 (2018).
- [62] B. Sapoval, T. Gobron, and A. Margolina, Vibrations of fractal drums, *Phys. Rev. Lett.* **67**, 2974 (1991).
- [63] M. L. Lapidus and M. M. H. Pang, Eigenfunctions of the

- Koch snowflake domain, *Commun. Math. Phys.* **172**, 359 (1995).
- [64] C. Even, S. Russ, V. Repain, P. Pieranski, and B. Sapoval, Localizations in Fractal Drums: An Experimental Study, *Phys. Rev. Lett.* **83**, 726 (1999).
- [65] B. Daudert and M. L. Lapidus, Localization on Snowflake Domains, *Fractals* **15**, 255 (2007).
- [66] L. Banjai, Eigenfrequencies of fractal drums, *J. Comput. Appl. Math.* **198**, 1 (2007).
- [67] M. E. Muller, Some Continuous Monte Carlo Methods for the Dirichlet Problem, *Ann. Math. Statist.* **27**, 569 (1956).
- [68] B. B. Mandelbrot, *The Fractal Geometry of Nature* (Freeman, San Francisco, 1982).
- [69] B. Sapoval, *Fractals* (Additech, Paris, 1989).
- [70] J.-F. Gouyet, *Physics and fractal structures* (Paris/New York: Masson Springer, 1996).
- [71] D. ben Avraham and S. Havlin, *Diffusion and Reactions in Fractals and Disordered Systems* (Cambridge Univ. Press, 2000).
- [72] M. Filoche and B. Sapoval, Transfer Across Random versus Deterministic Fractal Interfaces, *Phys. Rev. Lett.* **84**, 5776 (2000).
- [73] E. Akkermans, G. V. Dunne, and A. Teplyaev, Physical consequences of complex dimensions of fractals, *EPL* **88**, 40007 (2009).
- [74] E. Akkermans, O. Bénichou, G. V. Dunne, A. Teplyaev, and R. Voituriez, Spatial log-periodic oscillations of first-passage observables in fractals, *Phys. Rev. E* **86**, 061125 (2012).
- [75] D. Sornette, Discrete-scale invariance and complex dimensions, *Phys. Rep.* **297**, 239-270 (1998).
- [76] F. Cagnetta, G. Gonnella, A. Mossa, and S. Ruffo, Strong anomalous diffusion of the phase of a chaotic pendulum, *EPL* **111**, 10002 (2015).
- [77] J. M. Luck, Revisiting log-periodic oscillations, *Physica A* **643**, 129821 (2024).
- [78] J. Brossard and R. Carmona, Can One Hear the Dimension of a Fractal, *Commun. Math. Phys.* **104**, 103 (1986).
- [79] M. L. Lapidus, Fractal Drum, Inverse Spectral Problems for Elliptic Operators and a Partial Resolution of the Weyl-Berry Conjecture, *Trans. Am. Math. Soc.* **325**, 465 (1991).
- [80] M. L. Lapidus and C. Pomerance, Counterexamples to the modified Weyl-Berry conjecture on fractal drums, *Math. Proc. Camb. Phil. Soc.* **119**, 167 (1996).
- [81] Z. Zhang, B. Wu, H. Zhang, S. Zhou, J. Guan, and Z. Wang, Determining global mean-first-passage time of random walks on Vicsek fractals using eigenvalues of Laplacian matrices, *Phys. Rev. E* **81**, 031118 (2010).